Magnetism in amorphous transition metals

Y. Kakehashi
Department of Physics, Hokkaido Institute of Technology, Teine-Maeda, Teine-ku, Sapporo 006, Japan
(Received 5 November 1990)

Overall features of magnetism in amorphous transition metals have been investigated on the basis of a finite-temperature theory of the local-environment effect. It is shown that the simple ferromagnetism of Fe, Co, and Ni is drastically changed by structural disorder; amorphous transition metals form spin glasses (SG's) for compositions near amorphous Fe ($6.7 \lesssim N \lesssim 7.35$), ferromagnets for compositions near amorphous Co ($7.35 \lesssim N \lesssim 9.0$), and paramagnetisms for compositions near amorphous Ni ($9.0 \lesssim N \lesssim 10.0$) where N is the number of d electrons. The SG is accompanied by formation of local ferromagnetic clusters for $N \gtrsim 7.2$, and shows reentrant behavior at the ferromagnetic boundary $N \approx 7.35$. The ferromagnetism in amorphous transition metals is shown to be well explained by the main-peak position in the noninteracting densities of states. It is found that structural disorder enhances the Curie temperatures (T_C) in the range $7.9 \lesssim N \lesssim 8.5$ as compared with bcc and fcc structures. These results explain recent experimental data for the SG in Fe-rich amorphous alloys and the high T_C in amorphous Co-Y alloys, but they are quite different from the early picture obtained for amorphous transition-metal–metalloid alloys.

I. INTRODUCTION

Magnetism in amorphous transition-metal alloys has been extensively investigated from both fundamental and technological points of view.[1–3] The most essential question from a fundamental viewpoint is whether or not structural disorder leads to a different type of magnetism in transition metals.

Early systematic investigations concerning this problem have been performed with use of amorphous transition-metal alloys containing considerable amount of metalloids, such as B and P. A typical example of Curie temperatures obtained by Mizoguchi[2] is shown in Fig. 1. The Curie temperatures are in general reduced equally by about a factor of 2 as compared with those in the crystalline alloys. The same trend is seen also in the magnetization-versus-concentration curves. These results were thought to reveal that the effect of structural disorder is a uniform reduction of ferromagnetism, and that the amorphous systems do not show magnetism characteristic of the structure.

With recent developments of amorphous transition-metal alloys with compositions close to those of pure metals,[3–7] the picture of magnetism in amorphous alloys has changed. When Saito *et al.*[5] and Coey *et al.*[6] investigated Fe-rich amorphous Fe_cZr_{1-c} ($0.40 \le c \le 0.93$) alloys, they found that amorphous Fe-Zr alloys form spin glasses (SG's) with high transition temperature (120 K) beyond 92 at. % Fe after disappearance of the ferromagnetism. A similar behavior has been found by Wakabayashi *et al.*[7] in amorphous Fe-La alloys. Fukamichi *et al.*[3] performed systematic investigations on amorphous Fe_cM_{1-c} (M = Y, Zr, La, Ce, and Lu) alloys. They showed that these alloys have the same spin-glass temperature T_g irrespective of the second elements M beyond 90 at. % Fe (see Fig. 2). This implies that the SG's for alloys with 90 at. % Fe or more are caused not by configurational disorder, but rather by structural disorder, suggesting that introduction of structural order causes amorphous pure iron to make the magnetic phase transition from a ferromagnet to a SG.

An unusual change in magnetism has also been found by Fukamichi, Goto, and Mizutani[8] in the amorphous Co_cY_{1-c} ($0.6 \le c \le 0.9$) alloys. They found that the Curie temperature (T_C) in amorphous structure are higher than in crystalline ones by as much as several hundred kelvins, as shown in Fig. 3. Extrapolating their data to the amorphous pure Co, they speculated that the Curie

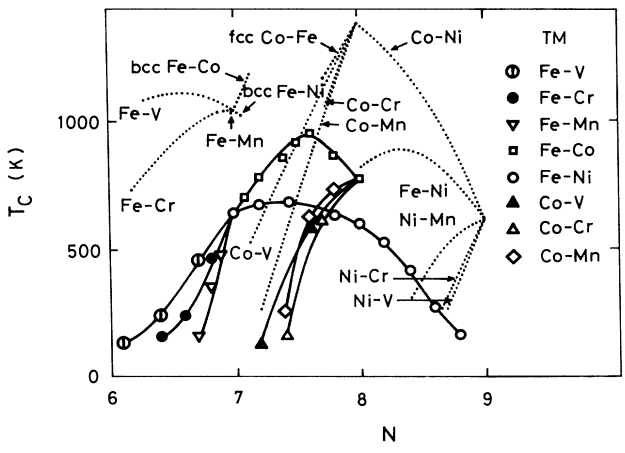

FIG. 1. Curie temperature (T_C) vs d-electron number (N) curves in amorphous transition-metal–metalloid alloys (T-$M)_{80}B_{10}P_{10}$ (solid curves) and crystalline transition-metal alloys T-M dotted curves (Ref. 2).

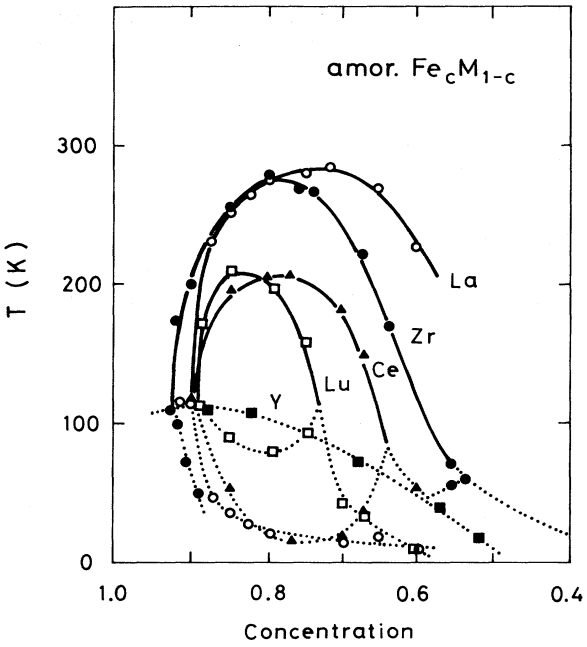

FIG. 2. Magnetic phase diagram showing the Curie temperatures (solid curves) and the spin-glass temperatures (dotted curves) in amorphous Fe_cM_{1-c} alloys (M =La, Zr, Ce, Lu, and Y) (Ref. 3).

temperature of amorphous pure Co can be as high as 1850 K, which is 450 K higher than that of the fcc Co.

The recent experimental results mentioned above suggest that structural disorder drastically changes the nature of magnetism in transition-metal alloys, in contradiction to the early picture as shown in Fig. 1. In the present paper, we clarify this problem from the theoretical point of view, and give a physical picture for a magnetism in amorphous transition metals by making use of a finite-temperature theory of local-environment effects (LEE's).[9]

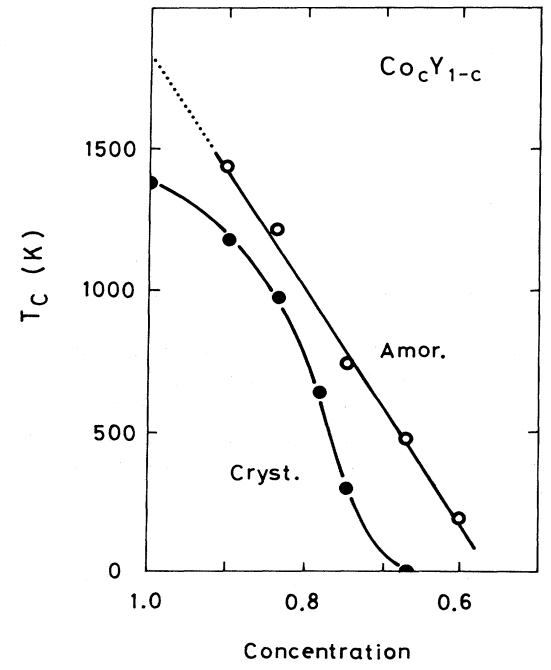

FIG. 3. Curie temperatures in crystalline (solid circles) and amorphous (open circles) Co_cY_{1-c} alloys (Ref. 8). Dotted line is an extrapolation to the amorphous pure Co.

Theoretical investigations for the itinerant-electron magnetism in amorphous alloys have not been made thus far, except for a few calculations for the ground state.[10,11] This is because a ground-state band theory, which self-consistently treated the local-moment (LM) configuration in the amorphous structure was lacking. In particular, it was impossible even at $T=0$ to examine the SG as found in Fe-rich amorphous alloys. Moreover, no theory that treats the finite-temperature magnetism of amorphous transition metals and alloys has hitherto been developed. The simple Stoner theory does not lead to a reasonable T_C, Curie-Weiss law in the susceptibility, and anomalously large specific heat at T_C in transition metals and alloys because of the lack of thermal spin fluctuations. In order to remove these difficulties, we have recently proposed a finite-temperature theory of LEE's for amorphous and liquid magnetic alloys.[9] The theory self-consistently determines the LM distribution in amorphous systems by means of the distribution-function method developed by Matsubara and Katsura.[12,13] The thermal spin fluctuations are taken into account by making use of the functional-integral method developed by Cyrot,[14] Hubbard,[15] and Hasegawa.[16] In Sec. II, we briefly review our theory of LEE's. (See Ref. 9 for details of the theory.)

The present work is a systematic investigation from the theoretical side, which throws light on metallic magnetism in the presence of structural disorder. We present the numerical results in Sec. III. In Sec. III A, we will examine overall features of the magnetism in amorphous transition metals as a function of the d-electron number N, and demonstrate that the main-peak position in the noninteracting densities of states (DOS) plays an important role in determining the basic properties of ferromagnetism in amorphous alloys. In Sec. III B, we investigate the SG for compositions near amorphous Fe. A part of this subsection has been published in previous papers.[9,17] An additional feature that we found is a cluster SG between the SG and ferromagnetic states. The magnetism of amorphous Co and Ni is presented in Sec. III C. The enhancement of T_C in amorphous Co is explained by the magnetic-energy gain associated with the main peak near the Fermi level in the noninteracting DOS. In the final section, Sec. IV, we summarize our results and discuss the magnetism of amorphous transition-metal alloys containing metalloids, as shown in Fig. 1, on the basis of our picture for amorphous pure transition metals.

II. FINITE-TEMPERATURE THEORY OF LEE'S

The magnetism in transition metals is well described by the degenerate-band Hubbard model with Hund's-rule coupling. We adopt this model and make use of the functional-integral method to take into account thermal

spin fluctuations.[18] In this method, the interacting Hubbard Hamiltonian is transformed into a one-electron Hamiltonian with time-dependent random exchange fields acting on each site. Within the static approximation in which the time dependence of the field variables is neglected, the central local moment is expressed as a classical average of the field variable ξ on the same site with respect to a free-energy functional.

Next, we introduce an effective medium $\mathcal{L}_\sigma^{-1}$ describing the thermal spin fluctuations into the diagonal part of the one-electron Hamiltonian, and expand the deviation from the effective medium in the energy functional with respect to the site. After making use of a molecular-field type of approximation for the surrounding field variables, we obtain an expression for the thermal average of the central local moment:[9]

$$\langle m_0 \rangle = \langle \xi \rangle = \frac{\int d\xi\, \xi e^{-\beta\Psi(\xi)}}{\int d\xi\, e^{-\beta\Psi(\xi)}} . \tag{2.1}$$

Here β denotes the inverse temperature.

The energy functional $\Psi(\xi)$ in Eq. (2.1) consists of the single-site energy $E(\xi)$, the atomic pair energies $\Phi_{0j}^{(a)}(\xi)$, and the exchange pair energies $\Phi_{0j}^{(e)}(\xi)$ in the effective medium.

$$\Psi(\xi) = E(\xi) + \sum_{j=1}^{z} \left[\Phi_{0j}^{(a)}(\xi) - \Phi_{0j}^{(e)}(\xi) \frac{\langle m_j \rangle}{x_j} \right] , \tag{2.2}$$

$$E(\xi) = \int d\omega\, f(\omega) \frac{D}{\pi} \mathrm{Im} \sum_\sigma \ln[L_\sigma^{-1}(\xi) - \mathcal{L}_\sigma^{-1} + F_{00\sigma}^{-1}] - N w_0(\xi) + \tfrac{1}{4}\tilde{J}\xi^2 , \tag{2.3}$$

$$\begin{bmatrix} \Phi_{0j}^{(a)}(\xi) \\ \Phi_{0j}^{(e)}(\xi) \end{bmatrix} = \tfrac{1}{2} \sum_{\nu=\pm} \begin{bmatrix} 1 \\ -\nu \end{bmatrix} \Phi_{0j}(\xi, \nu x_j) , \tag{2.4}$$

$$\Phi_{0j}(\xi, \nu x_j) = \int d\omega\, f(\omega) \frac{D}{\pi} \mathrm{Im} \sum_\sigma \ln[1 - F_{0j\sigma} F_{j0\sigma} \tilde{t}_{0\sigma}(\xi) \tilde{t}_{j\sigma}(\nu x_j)] , \tag{2.5}$$

$$\tilde{t}_{j\sigma}(\xi) = \frac{L_{j\sigma}^{-1}(\xi) - \mathcal{L}_\sigma^{-1}}{1 + (L_{j\sigma}^{-1}(\xi) - \mathcal{L}_\sigma^{-1}) F_{jj\sigma}} . \tag{2.6}$$

Here the summation on the right-hand side (RHS) of Eq. (2.2) is taken over z atoms on the well-defined nearest-neighbor (NN) shell. We have neglected the couplings between more distant atoms because of the rapid dumping in the disordered systems with increasing interatomic distance.[19] $\langle m_j \rangle$ and x_j are the thermal average and amplitude of LM on the neighboring site j. $f(\omega)$ in Eqs. (2.3) and (2.5) denotes the Fermi distribution function. D, N, and $\tilde{J}$ are the number of orbital degeneracy ($D=5$), d-electron number, and the effective exchange-energy parameter, respectively. The charge potential $w_j(\xi)$ in Eq. (2.3) is determined from the charge-neutrality condition on each site j. The locator for σ spin electrons, $L_{j\sigma}$, in Eqs. (2.3) and (2.6) is defined by

$$L_{j\sigma}^{-1}(\xi) = \omega + i\delta - \varepsilon^0 - w_j(\xi) + \tfrac{1}{2}\tilde{J}\xi\sigma + \mu , \tag{2.7}$$

where $\varepsilon^0 - \mu$ is the atomic level measured from the chemical potential μ, δ being an infinitesimal positive number.

The structural disorder appears in Eqs. (2.3) and (2.5) via the coherent Green's function, defined by

$$F_{ij\sigma} = [(\mathcal{L}_\sigma^{-1} - t)^{-1}]_{ij} , \tag{2.8}$$

where t denotes the transfer integral matrix t_{ij}.

In the present theory, the diagonal coherent Green's functions on the NN shell are approximated by the structural average:

$$[F_{jj\sigma}]_s = F_\sigma \equiv \int \frac{[\rho(\varepsilon)]_s}{\mathcal{L}_\sigma^{-1} - \varepsilon} d\varepsilon . \tag{2.9}$$

Here, $[\ ]_s$ means the structural average, and $\rho(\varepsilon)$ is the densities of states for noninteracting electrons in amorphous metals.

The coherent Green's functions $F_{00\sigma}$ and $F_{0j\sigma}$ ($=F_{j0\sigma}$) are obtained by making use of the Bethe approximation.[20]

$$F_{00\sigma} = \left[\mathcal{L}_\sigma^{-1} - \frac{\sum_{i=1}^{z} t_{i0}^2}{\mathcal{L}_\sigma^{-1} - \mathcal{S}_\sigma} \right]^{-1} , \tag{2.10}$$

$$F_{0j\sigma} = \frac{t_{j0}}{\mathcal{L}^{-1}{}_\sigma - \mathcal{S}_\sigma} F_{00\sigma} . \tag{2.11}$$

Here the self-energy $\mathcal{S}_\sigma$ describes an effective medium due to the structural disorder.

Equation (2.1) manifests that the central LM is determined by the surrounding LM's $\{\langle m_j \rangle\}$ and the squares of the transfer integrals $\{t_{j0}\}$. These quantities have the distributions $g(\langle m_j \rangle)$ and $p_s(y_j)$ in the amorphous systems, where $y_j = t^2{}_{j0} - [t^2{}_{j0}]_s$. The distribution of the central LM is then obtained from $g(\langle m_j \rangle)$ and $p_s(y_j)$ via Eq. (2.1). Since it is identical with the surrounding ones, we obtain an integral equation for the distribution function as follows:

$$g(M) = \int \delta(M - \langle m_0 \rangle) \prod_{j=1}^{z} [p_s(y_j) dy_j g(m_j) dm_j] . \tag{2.12}$$

By making use of the decoupling approximation on the RHS of Eq. (2.12), we obtain the self-consistent equations for $[\langle m \rangle]_s$ and $[\langle m \rangle^2]_s$:

$$\left.\begin{matrix}[\langle m\rangle]_s \\ [\langle m\rangle^2]_s\end{matrix}\right\}=\sum_{n=0}^{z}\Gamma(n,z,\tfrac{1}{2})\sum_{k=0}^{n}\sum_{l=0}^{z-n}\Gamma(k,n,q)\Gamma(l,z-n,q)\times\left\{\begin{matrix}\langle\xi\rangle_{nkl} \\ \langle\xi\rangle^2_{nkl}\end{matrix}\right., \tag{2.13}$$

$$\langle\xi\rangle_{nkl}=\frac{\int d\xi\,\xi e^{-\beta\Psi_{nkl}(\xi)}}{\int d\xi\, e^{-\beta\Psi_{nkl}(\xi)}}\ , \tag{2.14}$$

$$\Psi_{nkl}(\xi)=E_n(\xi)+n\Phi^{(a)}_{-n}(\xi)+(z-n)\Phi^{(a)}_{+n}(\xi)-[(2k-n)\Phi^{(e)}_{-n}(\xi)+(2l-z+n)\Phi^{(e)}_{+n}(\xi)]\frac{[\langle m\rangle^2]^{1/2}_s}{x}\ , \tag{2.15}$$

$$q=\tfrac{1}{2}\left[1+\frac{[\langle m\rangle]_s}{[\langle m\rangle^2]^{1/2}_s}\right]. \tag{2.16}$$

In the present approximation, the atomic local environment is described by a contraction or a stretch of the NN atomic distance by $[(\delta R)^2]^{1/2}_s$ on the NN shell. Both atomic and spin configurations are expressed by the binomial distribution function $\Gamma(k,n,q)$ defined by $[n!/k!(n-k)!]q^k(1-q)^{n-k}$. Thus the LM $\langle\xi\rangle_{nkl}$ and energy $\Psi_{nkl}(\xi)$ are specified by n (the number of contracted atoms on the NN shell), k (the number of up spins on the contracted atoms), and l (the number of up spins on the $z-n$ streched atoms). The associated energy functionals $E_n(\xi)$ and $\Phi^{(a)}_{+n}(\xi)$ $[\Phi^{(a)}_{-n}(\xi)]$ in Eq. (2.15) mean the single-site energy and the atomic pair energy for the contracted (stretched) pair in the local environment n. The exchange pair energies $\Phi^{(e)}_{\pm n}(\xi)$ are defined in the same way.

The energy functionals $\Psi_{nkl}(\xi)$ contain unknown parameters of the effective media $\mathcal{S}_\sigma$ and $\mathcal{L}_\sigma^{-1}$. The former is determined so that the structural average of $F_{00\sigma}$ [Eq. (2.10)] is equal to the exact one [Eq. (2.9)]:

$$\sum_{\nu=\pm}\tfrac{1}{2}[\mathcal{L}_\sigma{}^{-1}-z[t^2_{j0}]_s\left[1+\nu\frac{[(\delta t^2{}_{j0})^2]^{1/2}_s}{\sqrt{z}\,[t^2{}_{j0}]_s}\right](\mathcal{L}_\sigma{}^{-1}-\mathcal{S}_\sigma)^{-1}]^{-1}=F_\sigma\ . \tag{2.17}$$

Here the average transfer integral $[t^2{}_{j0}]_s$ is obtained from the input DOS as follows:

$$z[t^2{}_{j0}]_s=\int(\varepsilon-\varepsilon_0)^2[\rho(\varepsilon)]_s d\varepsilon\ . \tag{2.18}$$

The ratio $[(\delta t^2_{j0})^2]^{1/2}_s/[t^2_{j0}]_s$ is related with the fluctuation of the NN atomic distance as follows:

$$[(\delta t^2_{j0})^2]^{1/2}_s/[t^2_{j0}]_s=2\kappa\frac{[(\delta R)^2]^{1/2}_s}{[R]_s}\ . \tag{2.19}$$

Here, $t(R)\propto R^{-\kappa}$ (with $\kappa=3.8$) is assumed.[21,22]

The effective medium $\mathcal{L}_\sigma^{-1}$ is determined from the coherent-potential approximation (CPA) condition,[23,24]

$$\sum_\nu\tfrac{1}{2}\left[1+\nu\frac{[\langle\xi\rangle]_s}{[\langle\xi^2\rangle]^{1/2}_s}\right]\{L_\sigma^{-1}(\nu[\langle\xi^2\rangle]^{1/2}_s)-\mathcal{L}_\sigma^{-1}+F_\sigma^{-1}\}^{-1}=F_\sigma\ . \tag{2.20}$$

Since $[\langle\xi\rangle]_s$ and $[\langle\xi^2\rangle]_s$ in Eq. (2.20) includes again $[\langle m\rangle]_s$ and $[\langle m\rangle^2]_s$ via Eqs. (2.15) and (2.16), one has to solve Eqs. (2.13), (2.17), and (2.20) self-consistently to obtain $[\langle m\rangle]_s$, $[\langle m\rangle^2]_s$, $\mathcal{S}_\sigma$, and $\mathcal{L}^{-1}{}_\sigma$.

Apparently, the theory describes itinerant-electron SG's ($[\langle m\rangle]_s=0$ and $[\langle m\rangle^2]_s\neq0$). The transition temperature T_g has been shown to reduce to the well-known formula $T_g=\sqrt{z}\,|\mathcal{J}|$ in the LM limit and the $\pm\mathcal{J}$ model.[25,26] Here, $\mathcal{J}$ denotes the exchange coupling constant between the LM's.

The input parameters are the d-electron number N, the effective exchange-energy parameter $\tilde{J}$, the DOS $[\rho(\varepsilon)]_s$, and the fluctuation in the interatomic distance $[(\delta R)^2]^{1/2}{}_s/[R]_s$. In the following numerical calculations, we adopted $[(\delta R)^2]^{1/2}{}_s/[R]_s=0.06$, which is consistent with those estimated from the width of the first peak in the theoretical[27] and experimental[28] pair-distribution functions for amorphous Fe.

III. NUMERICAL RESULTS

A. Systematic variations in the magnetic moments and Curie temperatures

The first step to achieve an understanding of magnetism in amorphous metals is to examine the electronic structure. We show, in Fig. 4, the input DOS $[\rho(\varepsilon)]_s$ for amorphous Fe,[29] bcc Fe,[29] and fcc Fe.[30] An important feature of the amorphous Fe DOS is that the main peak near the top of the d band lies just between those of the bcc Fe DOS and the fcc Fe DOS. Fujiwara[10] pointed out that uniform ferromagnetism is not expected in amorphous Fe because of this change of the main peak due to structural disorder. If we adopt the same argument, we find ferromagnetism in amorphous Co because of the location of the Fermi level near the main peak, and paramagnetism or weak ferromagnetism in amorphous pure Ni. These predictions are based on a rough estimate of the Stoner criterion assuming the uniform magnetization. Since the LM's generally depend on their local environments, one has to perform numerical calculations based on our theory of LEE to examine the existence of ferromagnetism. The results of the calculations for the magnetization curves are presented in Fig. 5. Here we adopted the effective exchange energy parameter for Fe ($\tilde{J}=0.059045$ Ry) and the DOS in Fig. 4, and varied the d-electron number to reveal qualitative features of fer-

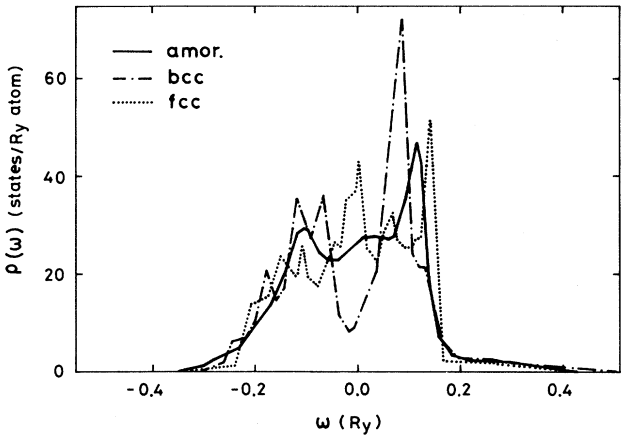

FIG. 4. The input densities of states (DOS) for the amorphous (solid curve) (Ref. 29), bcc (dot-dashed curve) (Ref. 29), and fcc (dotted curve) (Ref. 30) structures.

romagnetism in $3d$ transition metals.

Calculated spontaneous magnetization for amorphous structure occurs near compositions around Ni, and rapidly decrease near compositions around Fe with decreasing d-electron number. The curve explains well the average-d-electron-number dependence of the magnetization data in amorphous (Fe-M)$_{90}$Zr$_{10}$ (M=Mn, Co, and Ni) alloys.[31] A characteristic feature of the amorphous transition metals is that ferromagnetism is stable near compositions around Co (N=8.0), while the bcc (fcc) ferromagnetism is stable near compositions around Fe (Ni). In other words, it may safely be said that the structural disorder enhances ferromagnetism around the region where both bcc and fcc structures show ferromagnetic instability. The stable regions correspond to d-electron numbers having the Fermi level at the main peak in the DOS of each structure, as indicated by the arrows in Fig. 5. This verifies that the magnetic-energy gain due to the main peak near the Fermi level is responsible for ferromagnetism even in the amorphous structure.

Recently, Dumpich *et al.*[32] found that fcc $Fe_{68}Ni_{32}$ films with broad x-ray (111) intensity peak show a magnetization ($2.4\mu_B$) larger than that expected from the Slater-Pauling curve, while annealed films with a narrow x-ray intensity peak show a small magnetization ($1.4\mu_B$) which coincides with that found in bulk Fe-Ni alloys. Although they attributed their data to the existence of the high-spin state in the Weiss model,[33] which has recently been discussed on the basis of the ground-state band calculations,[34] we interpret them as the enhancement of ferromagnetism due to structural disorder as found in the present calculation, because the broadening of the x-ray intensity peak indicates a disturbance of the fcc structure.

The SG solutions due to the structural disorder is a striking feature in our theoretical calculations. The solutions exist even around Co (N=8.0) as shown by the dashed curves in Fig. 5. But the SG phase is realized after the disappearance of ferromagnetism, because the ferromagnetic-energy gain is generally larger than the SG. The SG solutions around N=6.0 are also unrealistic because the antiferromagnetism specified by a site-dependent effective medium is expected to be stabilized there. In fact, we found that all the NN magnetic couplings become antiferromagnetic in the region $N \lesssim 6.7$, irrespective of the local environments. It turns out that the SG is realized around the amorphous Fe.

The minimum of the order parameter $[\langle m \rangle^2]^{1/2}_s$ at

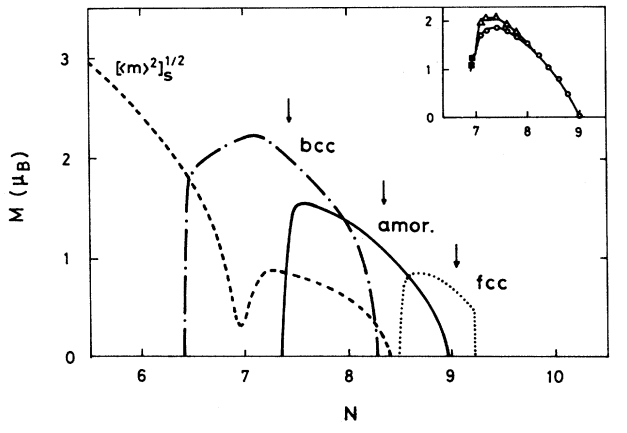

FIG. 5. Calculated magnetization vs d-electron number curves at 75 K for the amorphous (solid curve), bcc (dot-dashed), and fcc (dotted curve) structures. Effective exchange-energy parameter is fixed to the amorphous Fe ($\tilde{J}$=0.059 Ry). Dashed curve shows the spin-glass (SG) order parameter. The d-electron numbers integrated up to the main peak of each DOS in Fig. 4 are indicated by the arrows. The inset shows the experimental data for amorphous (Fe-M)$_{90}$Zr$_{10}$ alloys (Ref. 31). Here, M=Mn (■), Co (△), and Ni (○).

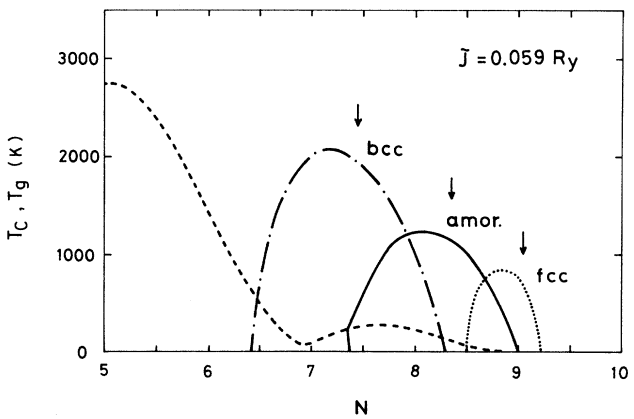

FIG. 6. Curie temperature vs d-electron number curves calculated with use of the same input parameters as in Fig. 5. The SG temperatures are shown by dashed curve. The d-electron numbers showing the peak position in the input DOS are indicated by the arrows.

$N=6.95$ is caused by a change in sign of the average magnetic couplings with decreasing d-electron number. Details of the SG problems will be discussed in Sec. III B.

Systematic variation of the Curie temperature, as well as the SG temperature, is presented in Fig. 6. Calculated Curie temperature for bcc Fe is 2020 K. This is twice the experimental value [1040 K (Ref. 35)] because of the molecular-field-type approximation.[36] It is seen that the maximum T_C roughly corresponds to the main-peak position in the noninteracting DOS. This fact indicates that the Curie temperatures in $3d$ transition metals are mainly determined by the magnetic-energy gain associated with the main peak in each DOS.

As has already been mentioned, the antiferromagnetic solutions are expected to be more stable than the SG solution in the region $N \lesssim 6.7$. Since the SG temperatures amount to 1000 K in this region, we speculate that the Néel temperatures in amorphous transition metals around $N=6.0$ would be enhanced as compared with the fcc ones. This is because the spin frustrations in the fcc structure are mostly destroyed by structural disorder. In fact, such an enhancement is seen in the SG temperature T_g; T_g's in Fe-rich amorphous alloys are as high as 120 K (see Fig. 2), while those in the fcc $(Fe_cNi_{1-c})_{92}C_8$ and $(Fe_cNi_{1-c})_{80}Cr_{20}$ alloys[37,38] are reported to be less than 30 K.

B. Spin glasses around amorphous Fe

We have discussed the magnetism of amorphous Fe in previous papers.[9,17] It was concluded that the amorphous Fe shows itinerant-electron SG behavior because of the nonlinear magnetic coupling and the LEE's on the amplitude of LM due to structural disorder. In this subsection we argue in favor of formation of spin glasses around Fe in more detail.

In Fig. 7 we show the calculated magnetic phase diagram around $N=7.0$. Calculated SG temperatures are 100–200 K around $N=7.0$, which are consistent with the experimental data (≈ 120 K) in Fe-rich amorphous alloys around 90 at. % Fe (Ref. 3).

As has been discussed in a previous paper, the amorphous Fe ($N=7.0$) shows the anomalous nonlinear magnetic couplings; the Fe LM's with large amplitude ferromagnetically couple with the neighboring LM's, while the Fe LM's with small amplitude antiferromagnetically couple with the neighboring ones. This is seen from the energy functionals in Fig. 8. [Note that the exchange pair energies $-\Phi^{(e)}_{+n}(\xi)$ mean the magnetic pair-energy gain for the central LM ξ when the neighboring LM with average amplitude x points up, as seen from Eq. (2.2).] Since the amplitude of LM depends strongly on the surrounding environments, as seen from the various minimum points of the single-site energy $E_n(\xi)$ in Fig. 8, the sign of the magnetic couplings changes with the local environments (see Fig. 9). This leads to SG behavior in amorphous Fe.

As the d-electron number is increased in the SG region, the nonlinear magnetic couplings between the NN LM's disappear in the region $N \gtrsim 7.2$, as shown in Fig. 10. Nevertheless, SG behavior remains in the region $7.2 \lesssim N \lesssim 7.385$. This paradoxical situation may be understood from the following argument.

Since the NN couplings are ferromagnetic, the LM's certainly form ferromagnetic clusters. If ferromagnetic long-range order in these clusters developed, the effective medium would have a polarization consistent with NN ferromagnetic couplings. However, we found that the antiferromagnetic couplings occur between the central LM and the effective medium, once the medium is polarized. The central LM is then reversed, and therefore the ferromagnetic order cannot increase (see Fig. 11).

The resulting SG is accompanied by formation of ferromagnetic clusters in the region $7.2 \lesssim N < 7.385$. Thus

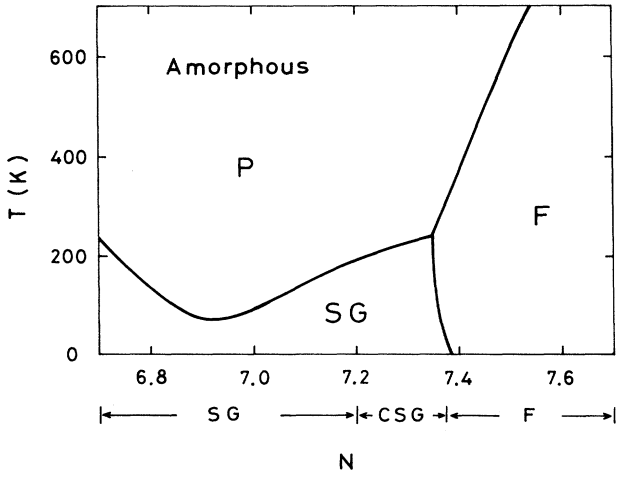

FIG. 7. Magnetic phase diagram around amorphous Fe showing the ferromagnetic (F), paramagnetic (P), and the spin-glass (SG) states. The cluster SG (CSG) phase is expected in the region $7.2 \lesssim N < 7.385$.

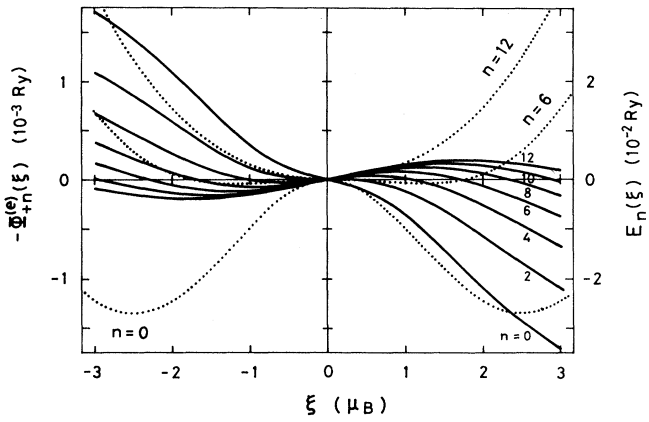

FIG. 8. Single-site energy [$E_n(\xi)$, dotted curves] and exchange pair energy [$-\Phi^{(e)}_{+n}(\xi)$, solid curves] for $N=7.0$ at $T=35$ K in various environments (n, number of contracted atoms on the NN shell).

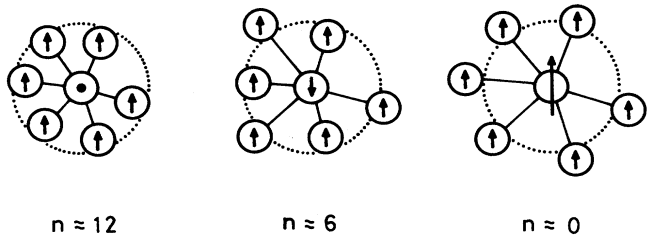

FIG. 9. Schematic representation showing the local-environment effect on the central local moment (LM) around amorphous Fe ($N=7.0$). n denotes the number of contracted atoms on the NN shell.

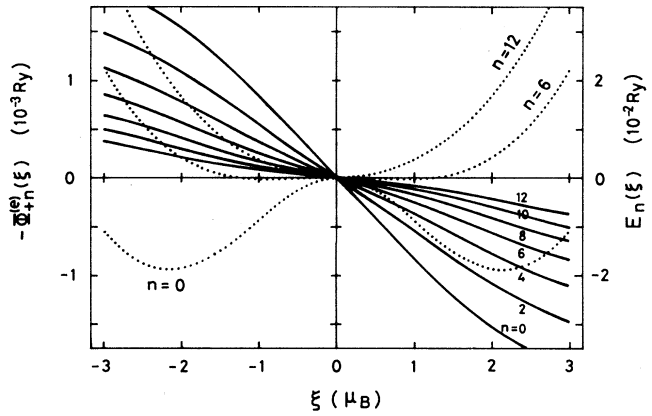

FIG. 10. The same as in Fig. 8 but for $N=7.365$.

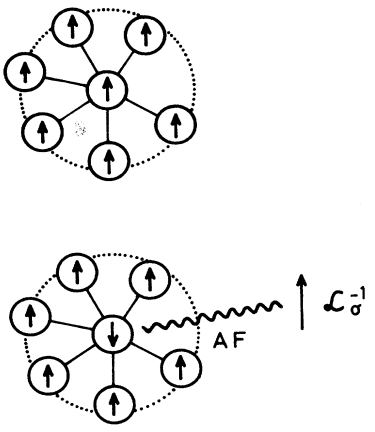

FIG. 11. Schematic representation showing the formation of the cluster SG. The short-range ferromagnetic couplings form ferromagnetic clusters. But the long-range antiferromagnetic couplings between the central LM and the polarized medium ($\mathcal{L}_\sigma^{-1}$) suppress the ferromagnetism.

we call it the cluster SG phase. Although the present theory cannot treat clusters extending beyond the NN shell, what really happens is probably that the size of the ferromagnetic clusters increases with increasing electron number, so that the clusters finally reach the ferromagnetic state after a second-order transition.

The LM distributions in the SG region are presented in Fig. 12. They range from $-2.5\mu_B$ to $2.5\mu_B$. The narrowing of the distribution around $N=7.0$ corresponds to the vanishing of averaged magnetic couplings. The SG's in this region are mostly created by fluctuations in magnetic couplings due to structural disorder.

The calculated LM distributions are consistent with the broad internal-field distributions in amorphous $Fe_{93}Zr_7$, $Fe_{92}La_8$, and $Fe_{92}Hf_8$ alloys.[6,7,39] But for a detailed comparison with the experimental data, one needs the distribution of the coupling constants between the nuclear spin and the surrounding LM's in a phenomenological expression for the internal field.

In the present calculations, the reentrant SG appears in the narrow region $7.350 \lesssim N \lesssim 7.385$. The temperature dependence of the magnetization and the SG order parameter in this region is presented in Fig. 13. Although we treat itinerant-electron systems, both curves are similar to those expected from the Sherrington-Kirkpartrik model,[26] in which the Ising spins interact through infinite-ranged exchange interactions with a Gaussian

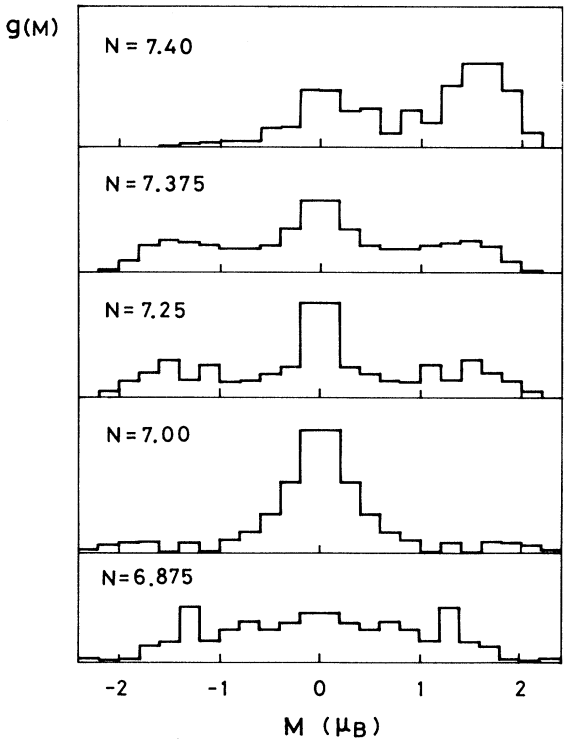

FIG. 12. The LM distributions [$g(M)$] around amorphous Fe at 35 K. N denotes the d-electron number.

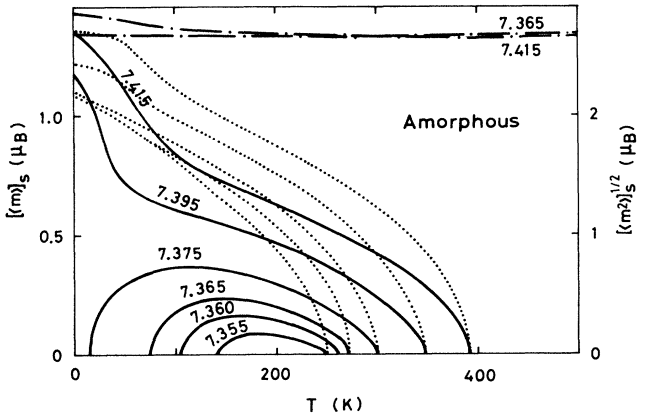

FIG. 13. Magnetization ($[\langle m \rangle]_s$, solid curves) and the SG order parameter ($[\langle m \rangle^2]^{1/2}_s$, dotted curves) as a function of temperature around the reentrant regime. The curves below 35 K are extrapolated. The numbers in the figure indicate the d-electron number N. The amplitudes of LM's are also shown by the dot-dashed curves.

distribution.

The temperature dependence of the LM distribution in the reentrant region is shown in Fig. 14. The existence of the paramagnetic component [i.e., g ($M=0$)] at low temperatures indicates the Curie-Law behavior in the susceptibilities. The transition from the SG to the ferromagnet with rising temperature is accompanied by a reversal of the LM's with four or five contracted NN atoms. This change is seen in Fig. 4 as a decrease in the weight around $M=-1.5\mu_B$, and an increase around $M=0.5\mu_B$ at $T=0.37T_c$.

According to our analysis for $N=7.365$, the average exchange coupling constants,[40] defined by $\mathcal{J}=[\Phi^{(e)}(x)-\Phi^{(e)}(-x)]/2$, increase from $\mathcal{J}=1.78\times10^{-4}$ (0.65×10^{-4}) Ry at 0 K to $\mathcal{J}=3.20\times10^{-4}$ (1.2×10^{-4}) Ry at T_C for the contracted (stretched) pairs. This indicates that the short-range ferromagnetic interactions are enhanced as compared with the long-range antiferromagnetic interactions, so that the ferromagnetism appears with increasing temperature.

Experimentally, reentrant behavior is found in the Fe-rich amorphous alloys in the wide range of Fe concentrations as shown in Fig. 2. A qualitative feature of the reentrant SG's around 90 at. % Fe is expected to be explained by the present calculations, because the effect of the structural disorder should be much stronger than that of the configurational disorder in this region, though the latter becomes more important for lower Fe concentrations. A detailed comparison of our results with the experimental data in the reentrant regime will be presented elsewhere.[41]

C. Amorphous Co and Ni, and enhancement of T_C

The structure of amorphous Co is considered to be essentially the same as in amorphous Fe. Thus we scaled the d-band widths W of the input DOS (Fig. 4) with use of the ratio $W(\mathrm{Co})/W(\mathrm{Fe})=0.441/0.393$ in the fcc structure,[30] and calculated the magnetic properties of Co in the bcc, fcc, and amorphous structures.

Numerical examples of the DOS in various environments are shown in Figs. 15 and 16. Here, we adopted the parameters $N=8.1$, and $\tilde{J}=0.100$ Ry. In the fer-

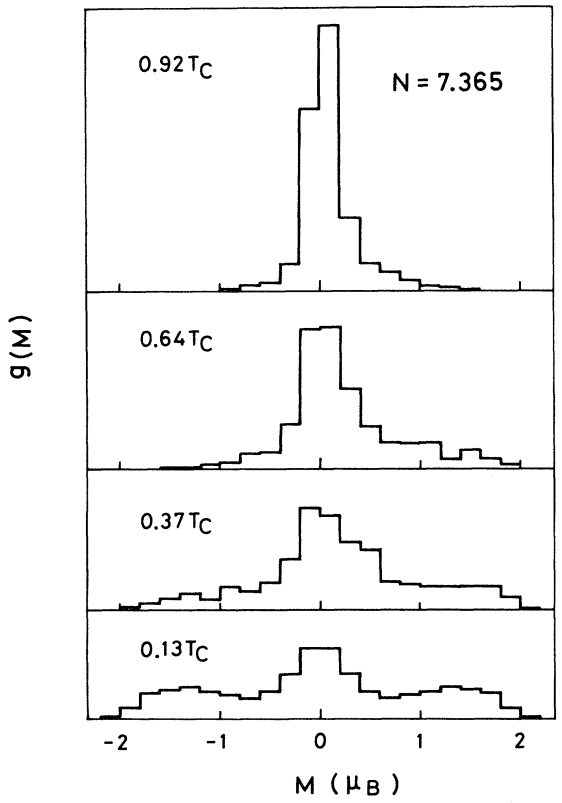

FIG. 14. Temperature variation of the LM distribution for $N=7.365$.

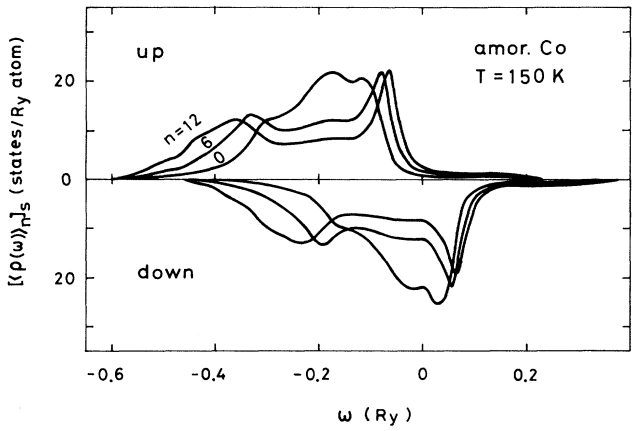

FIG. 15. Averaged up and down DOS of the ferromagnetic amorphous Co in various environments (n).

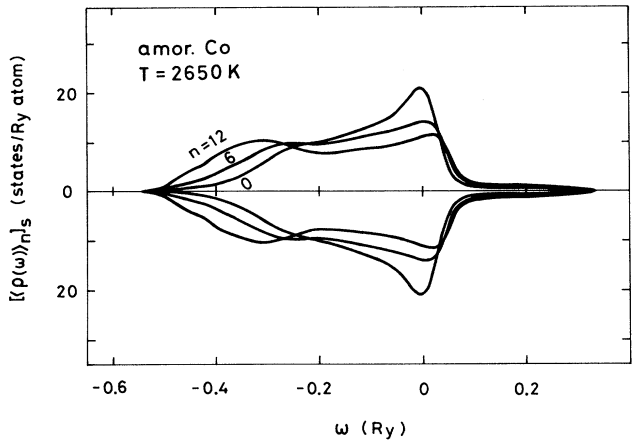

FIG. 16. Averaged DOS of the paramagnetic amorphous Co in various environments.

romagnetic state, the up-spin DOS are below the Fermi level because of the strong ferromagnetism. The up and down DOS for isolated atoms ($n=0$) form a narrow band, while those with the environments $n \geq 6$ show the double-peak structure. In the paramagnetic state, the main peaks of the up and down DOS are located at the Fermi level, suggesting the large magnetic-energy gain even above T_C. One of the important differences between the amorphous Fe and Co is that the DOS for the isolated Co ($n=0$) does not show a clear exchange splitting because of larger d-electron number; the DOS shows a single peak around the Fermi level.

The calculated magnetization-versus-temperature curves are presented in Fig. 17. In the present choice of parameters, the ground-state magnetizations are $1.51\mu_B$ for bcc, Co $1.69\mu_B$ for fcc Co, and $1.57\mu_B$ for amorphous Co. These are in approximate agreement with the experimental values $1.53\mu_B$ (Ref. 42), $1.74\mu_B$ (Ref. 43), and $1.72\mu_B$ (Ref. 8), respectively. The calculated T_C are 2640 K for bcc Co, 2480 K for fcc Co, and 2970 K for amorphous Co, as compared with the experimental values 1500 K (extrapolated value),[44] 1388 K,[45] and 1850 K (extrapolated value),[8] respectively. They are overestimated by a factor of 1.8 because of the molecular-field approximation.[36] The susceptibilities follow the Curie-Weiss law. The calculated effective Bohr magneton numbers are $2.25\mu_B$ for bcc Co, $2.39\mu_B$ for fcc Co, and $2.02\mu_B$ for amorphous Co. The experimental value for fcc Co is $3.15\mu_B$ (Ref. 46).

The calculated T_C of amorphous Co is 490 K higher than that of fcc Co. If we take into account a reduction factor of 1.8 due to the molecular-field-type approximation, we expect an enhancement by 300 K due to the amorphous structure in Co. This is consistent with the experimental speculation by Fukamichi, Goto, and Mizutani.[8] The enhancement of T_C is not very sensitive to the d-electron number, as shown in Fig. 18; the amorphous structure has a T_C higher than the bcc and fcc structure in the region $7.9 < N < 8.5$. Since the d-electron numbers showing the maximum T_C correspond well to those for the main-peak position in the noninteracting DOS, the high T_C in the amorphous Co is basically due to the magnetic-energy gain associated with the main peak of the DOS located around the Fermi level. In addition, it is also favorable to the relative enhancement of amorphous T_C that the magnetization for the fcc rapidly decrease near T_C.

The amorphous and fcc curves for T_C cross at $N=8.5$, as seen in Fig. 18. Although there is not direct experimental data for it, we point out that such a crossing of T_C is found in the concentration dependence of the Weiss

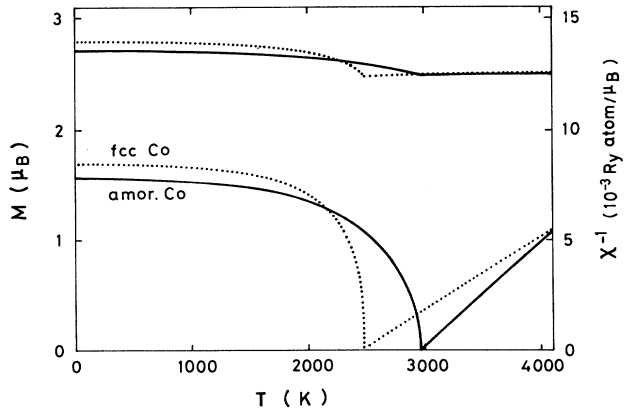

FIG. 17. Magnetizations, inverse susceptibilities, and amplitudes of LM's for the amorphous Co (solid curves) and fcc (dotted curves) Co ($N=8.1$ and $\tilde{J}=0.100$ Ry) as a function of temperature.

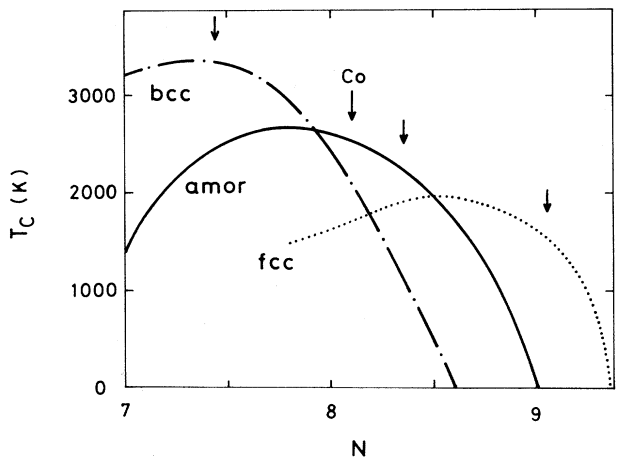

FIG. 18. Curie temperature around Co in the various structures. The d-electron numbers for Co ($N=8.1$) and the main-peak position in the input DOS are shown by arrows. The parameter $\tilde{J}=0.090$ Ry is used.

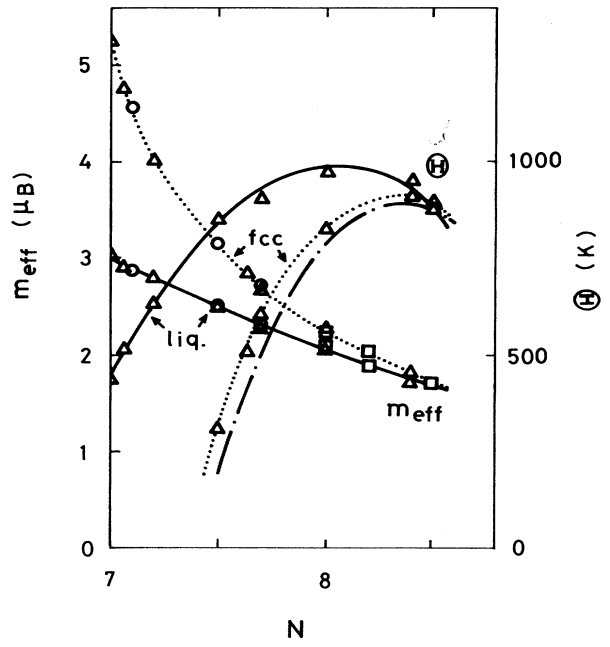

FIG. 19. Concentration dependence of the experimental effective Bohr magneton number (m_{eff}) and the Weiss constant (Θ) for the liquid (solid curves) and fcc (dotted curves) transition-metal alloys (Ref. 48): △, Fe-Ni, ○, Fe-Co; □, Co-Ni. The Curie temperatures for fcc Fe-Ni alloys are also shown by the dot-dashed curve.

constant in the paramagnetic susceptibilities of liquid and fcc transition-metal alloys,[47,48] (see Fig. 19). The data seem to support our result since the Weiss constants in the fcc Fe-Ni alloys are very close to the Curie temperatures, and, in addition, the liquid structure is similar to the amorphous one.

We also examined amorphous Ni with use of the DOS in Fig. 4, assuming $N=9.1$, and the scaling factor $W(\mathrm{Ni})/W(\mathrm{Fe})=0.364/0.393$ (Ref. 30). Figure 20 shows

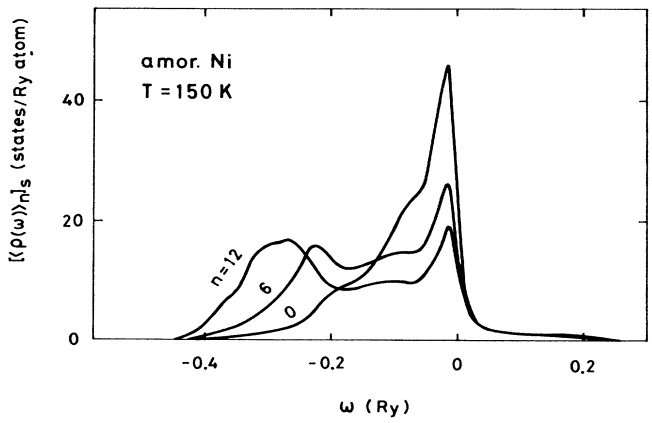

FIG. 20. Averaged DOS of the paramagnetic amorphous Ni in various environments.

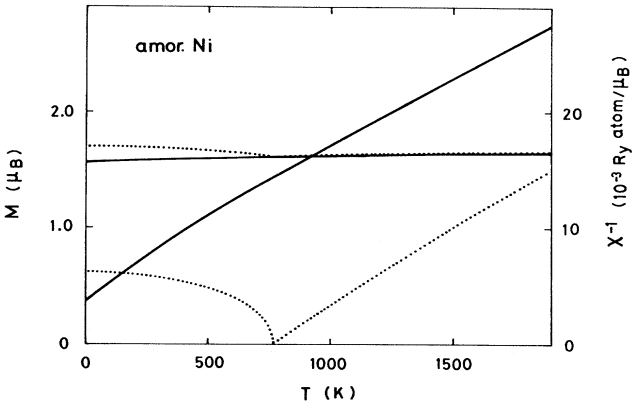

FIG. 21. The same as in Fig. 17, but for Ni ($N=9.1$, and $\tilde{J}=0.060$ Ry).

the LEE on the DOS in the paramagnetic state. It is seen that the main peak in the DOS for isolated atoms ($n=0$) shifts to the Fermi level because of the charge-neutrality condition, though the averaged DOS is almost the same as in amorphous Fe. The calculated magnetization and susceptibility are presented in Fig. 21 as a function of temperature. Amorphous Ni does not exhibit ferromagnetism in the present calculations since the main peak shifts to lower energy due to structural disorder. The calculated effective Bohr magneton number is $1.27\mu_B$ for amorphous Ni and $1.26\mu_B$ for fcc Ni, while the experimental value is $1.6\mu_B$ for fcc Ni.[49]

Experimental data for amorphous $Ni_{1-c}Y_c$ [$0.03<c<0.25$ (Ref. 50)] as well as amorphous $Ni_{1-c}La_c$ alloys,[51] suggest that amorphous pure Ni exhibits ferromagnetism in contradiction to the present calculation, although the Weiss constant (-435 K) obtained from the inverse susceptibility of liquid Ni (Ref. 47) suggests paramagnetism. In connection with this discrepancy, we have to take into consideration the following problems. First, the degree of structural disorder in amorphous Ni-Y alloys has not yet been examined experimentally. There is a possibility that the parameter $[(\delta R)^2]^{1/2}_s[R]_s$ is smaller than the 0.06 that we assumed in our calculation, so that ferromagnetism is realized in the experiment. It is highly desirable to examine the pair distribution function by means of x-ray techniques. Second, ferromagnetism around Ni is sensitive to the d-electron number, as seen from Fig. 18. It is not easy to determine the d-electron number in amorphous Ni with a precision under ± 0.1. Thus first-principles ground-state calculations are required to settle this problem.

IV. CONCLUSION AND DISCUSSION

We have presented overall features of magnetism in amorphous $3d$ transition metals on the basis of a finite-temperature theory of LEE's for amorphous and liquid systems. We have shown that magnetism in transition metals is drastically changed by structural disorder, and it is basically governed by the electronic structure in-

herent in the amorphous transition metals.

Ferromagnetism has been shown to be stabilized in amorphous transition metals in the region $7.35 \lesssim N \lesssim 9.0$. It is characterized by the main-peak position in the noninteracting averaged DOS, which is located just between the bcc and fcc DOS peaks. Since amorphous Fe has a Fermi level below the main peak, the ferromagnetism in bcc Fe is destroyed by the introduction of structural disorder. On the other hand, the Fermi level of amorphous Co is located at the peak of the input DOS, so that ferromagnetism is stabilized. The enhancement of the Curie temperature in amorphous Co is also attributed to the magnetic-energy gain associated with the Fermi level located at the peak. Ferromagnetism in fcc Ni is well known to be stabilized by a sharp peak, located at the Fermi level. When this peak is shifted down to lower energy by structural disorder, ferromagnetism is expected to be weakened. The present theory predicts that the paramagnetism would be accomplished in amorphous Ni if the degree of structural disorder is comparable to that in amorphous Fe.

The itinerant-electron SG are expected to be stabilized in the region $6.7 \lesssim N \lesssim 7.35$ by a competition between the ferromagnetic and antiferromagnetic couplings. The mechanism changes with d-electron numbers. The NN nonlinear magnetic couplings and the LEE on the amplitudes of LM's lead to coexistence of the ferromagnetic and antiferromagnetic couplings in the region $6.7 \lesssim N \lesssim 7.2$, so that the LM's are randomly frozen at low temperatures. However, in the region $7.2 \lesssim N \lesssim 7.35$, the NN couplings are ferromagnetic, irrespective of the local environments. But the long-range ferromagnetic order is suppressed because of the long-range antiferromagnetic couplings. The SG's are then accompanied by formation of ferromagnetic clusters. With increasing d-electron number, the size of the clusters is expected to increase, so that finally ferromagnetism is achieved after a second-order phase transition.

The physical picture for the magnetism in amorphous pure transition metals presented in this paper provides us with a basis for understanding various magnetic properties of amorphous transition-metal alloys. For example, magnetism in amorphous transition-metal–metalloid alloys as shown in Fig. 1 may be explained as follows. According to the electronic-structure calculations by Fujiwara[10] for amorphous $Fe_{80}B_{20}$ alloys, the effect of metalloid addition is a d-band narrowing due to the volume expansion and a shift toward lower energy of the main peak due to hybridization between the Fe d and the metalloid p states. The drastic change in magnetism with the introduction of metalloids is attributed to the latter, since the former simply enhances the ferromagnetism irrespective of the d-electron number. In fact, the Fermi energy moves to the main peak in the amorphous $Fe_{80}B_{10}P_{10}$ alloy because of the peak shift, so that ferromagnetism is recovered in amorphous Fe-rich metalloid alloys. The ferromagnetism in amorphous $Co_{80}B_{10}P_{10}$ alloys is weakened because the magnetic-energy gain is lost by the shift down of the main peak. The amorphous $Ni_{80}B_{10}P_{10}$ alloys, on the other hand, is not strongly influenced by the shift, because the peak in amorphous Ni is also located below the Fermi level. The resulting magnetization and Curie temperature curves are outwardly reduced as compared with those in crystalline transition-metal alloys.

Most of our results have as yet not been verified experimentally. More systematic experimental investigations for the amorphous $3d$ transition metals are needed to examine the physical picture presented here. In particular, amorphous Fe is expected to have an itinerant-electron SG caused only by structural disorder. The investigations for amorphous $(Fe\text{-}Ni)_{90}Zr_{10}$, $(Fe\text{-}Mn)_{90}Zr_{10}$, and $(Fe\text{-}Cr)_{90}Zr_{10}$ alloys might verify the magnetic phase diagram around amorphous Fe as shown in Fig. 7. Mössbauer experiments for these alloys are expected to provide us with important information concerning the LM distribution $g(M)$ as shown in Figs. 12 and 14. A recent neutron experiment[52] suggests a coexistence of propagating spin-wave excitations and spin-freezing phenomena in amorphous $Fe_{90}Zr_{10}$ alloys at low temperatures. Photoemission experiments might provide evidence for the main-peak shift due to structural disorder as seen in Fig. 4. Furthermore, simultaneous measurement of the pair distribution function in these experiments is indispensable to examine the degree of structural disorder. In a forthcoming paper, we will discuss other magnetic properties such as susceptibility, T-P phase diagram, and forced volume magnetostriction to establish the validity of our theory by comparing our results with more experimental data.

ACKNOWLEDGMENTS

The author would like to thank Dr. V. L. Moruzzi and Professor T. Fujiwara for sending him their DOS for γ Fe and amorphous Fe, respectively. He is also much indebted to Professor K. Fukamichi, Professor T. Goto, Dr. H. Komatsu, Professor M. Matsuura, Professor S. Murayama, and Professor H. Tange for valuable discussions. This work was supported by a Grant-in-Aid for Scientific Research from the Ministry of Education, Science, and Culture in Japan.

[1]See, for a review on recent development of amorphous magnetism, K. Moorjani and J. M. D. Coey, *Magnetic Glasses (Elsevier, Amsterdam, 1984);* T. Kaneyoshi, Amorphous Magnetism (CRC Press, Boca Raton, 1986); in *Proceedings of the 34th Annual Conference on Magnetism and Magnetic Materials, Boston, 1989,* edited by J. D. Adam, I. A. Beardsley, W. M. Saslow, and W. B. Yalon [J. Appl. Phys. **67**, Pt. II (1990)].

[2]T. Mizoguchi, in *Magnetism and Magnetic Materials—1976 (Joint MMM-Intermag Conference, Pittsburgh)* Partial Proceedings of the First Joint MMM–Intermag Conference, edited by J. J. Becker and G. H. Lander, AIP Conf. Proc. No. **34**, (AIP, New York, 1976), p. 286.

[3]K. Fukamichi, T. Goto, H. Komatsu, and H. Wakabayashi, in *Proceedings of Fourth International Conference on the Physics of Magnetic Materials, Warsaw, 1988,* edited by W. Gorkowski, K. Lachowicz, and H. Seymczak (World Scientific,

Singapore, 1989), p. 354.
[4]H. Hiroyoshi and K. Fukamichi, J. Appl. Phys. **53**, 2226 (1982).
[5]N. Saito, H. Hiroyoshi, K. Fukamichi, and Y. Nakagawa, J. Phys. F **16**, 911 (1986).
[6]J. M. D. Coey, F. Givord, A. Lienard, and J. P. Reboulat, J. Phys. F **11**, 2707 (1981); D. H. Ryan, J. M. D. Coey, E. Batalla, Z. Altonian, and J. O. Ström-Olsen, Phys. Rev. B **35**, 8630 (1987).
[7]H. Wakabayashii, K. Fukamichi, H. Komatsu, T. Goto, T. Sakakibara, and K. Kuroda, in *Proceedings of the International Symposium on Physics of Magnetic Materials, City, 1986,* (World Scientific, Singapore, 1987), p. 342.
[8]K. Fukamichi, T. Goto, and U. Mizutani, IEEE Trans. Magn. MAG-**23**, 3590 (1987).
[9]Y. Kakehashi, Phys. Rev. B **41**, 9207 (1990).
[10]T. Fujiwara, J. Non-Cryst. Solids **61&62**, 1039 (1984).
[11]S. Krompiewski, U. Krey, and H. Ostermeier, J. Magn. Magn. Mater. **69**, 117 (1987); S. Krompiewski, U. Krey, U. Krauss, and H. Ostermeier, *ibid.* **73**, 5 (1988).
[12]F. Matsubara, Prog. Theor. Phys. **52**, 1124 (1974).
[13]S. Katsura, S. Fujiki, and S. Inawashiro, J. Phys. C **12**, 2839 (1979).
[14]M. Cyrot, J. Phys. (Paris) **33**, 25 (1972).
[15]J. Hubbard, Phys. Rev. B **19**, 2626 (1979); **20**, 4584 (1979); **23**, 5974 (1981).
[16]H. Hasegawa, J. Phys. Soc. Jpn. **46**, 1504 (1979); **49**, 178 (1980).
[17]Y. Kakehashi, Phys. Rev. B **40**, 11 059 (1989).
[18]Y. Kakehashi, Phys. Rev. B **34**, 3243 (1986).
[19]A. Bieber and F. Gautier, Solid State Commun. **39**, 149 (1981); T. Oguchi, K. Terakura, and N. Hamada, J. Phys. F **13**, 145 (1983).
[20]H. Miwa, Prog. Theor. Phys. **52**, 1 (1974).
[21]V. Heine, Phys. Rev. **153**, 673 (1967).
[22]U. K. Poulsen, J. Kollár, and O. K. Andersen, J. Phys. F **6**, L241 (1976).
[23]P. Soven, Phys. Rev. **156**, 809 (1967); B. Velický, S. Kirkpartick, and H. Ehrenreich, *ibid.* **175**, 747 (1968).
[24]H. Shiba, Prog. Theor. Phys. **46**, 77 (1971).
[25]S. F. Edwards and P. W. Anderson, J. Phys. F **5**, 965 (1975).
[26]D. Sherrington and S. Kirkpatrick, Phys. Rev. Lett. **35**, 1972 (1975).
[27]R. Yamamoto and M. Doyama, J. Phys. F **9**, 617 (1979).
[28]M. Matsuura, H. Wakabayashi, T. Goto, H. Komatsu, and K. Fukamichi, J. Phys. Condens. Matter **1**, 2077 (1989).
[29]T. Fujiwara, Nippon Butsuri Gakkaishi **40**, 209 (1985).
[30]V. L. Moruzzi, J. F. Janak, and A. R. Williams, *Calculated Electronic Properties of Metals* (Pergamon, New York, 1978).
[31]T. Masumoto, S. Ohnuma, K. Shirakawa, M. Nose, and K. Kobayashi, J. Phys. (Paris) Colloq. **41**, C8-686 (1980).
[32]G. Dumpich, E. Becker, K. Schletz, W. Stamm, W. Keune, W. Kiauka, and S. Murayama, J. Magn. Magn. Mater. **74**, 237 (1988).
[33]R. J. Weiss, Proc. Phys. Soc. London, Sect. A **82**, 281 (1963).
[34]D. M. Roy and D. G. Pettifor, J. Phys. F **7**, L183 (1977); D. Bagayoko and J. Callaway, Phys. Rev. B **28**, 5419 (1983); V. L. Moruzzi, P. M. Marcus, K. Schwarz, and P. Mohn, Phys. Rev. B **34**, 1784 (1983).
[35]A. Arrot and J. E. Noakes, Phys. Rev. Lett. **19**, 786 (1967).
[36]Y. Kakehashi, J. Phys. (Paris) Colloq. **49**, C8-73 (1988).
[37]S. Ishio, K. Nushiro, and M. Takahashi, J. Phys. F **16**, 1093 (1986).
[38]M. Acet, W. Stamm, H. Zahres, and E. F. Wassermann, J. Magn. Magn. Mater. **68**, 233 (1987).
[39]D. H. Ryan, J. M. D. Coey, and J. O. Ström-Olsen, J. Magn. Magn. Mater. **67**, 148 (1987).
[40]Y. Kakehashi, Phys. Rev. B **38**, 474 (1988).
[41]Y. Kakehashi (unpublished).
[42]G. A. Prinz, Phys. Rev. Lett. **54**, 1051 (1985).
[43]M. J. Besnus, A. J. P. Meyer, and R. Berniger, Phys. Lett. **32**, 192 (1970).
[44]H. C. Van Elst, B. Lubach, and G. J. Van Den Berg, Physica **28**, 1297 (1962).
[45]R. V. Colvin and S. Arajs, J. Phys. Chem. Solids **26**, 435 (1965).
[46]M. Fallot, J. Phys. Radium **5**, 153 (1944).
[47]Y. Nakagawa, J. Phys. Soc. Jpn. **11**, 855 (1956); **12**, 700 (1957).
[48]I. Renz and S. Methfessel, J. Phys. (Paris) Colloq. **49**, C8-119 (1988).
[49]W. Sucksmith and R. R. Pearce, Proc. R. Soc. London, Sect. A **167**, 189 (1938).
[50]A. Lienard and J. R. Rebouillat, J. Appl. Phys. **49**, 1680 (1978).
[51]K. Fukamichi (private communication).
[52]J. A. Fernandez-Baca, J. J. Rhyne, G. E. Fish, M. Hennion, and B. Hennion, J. Appl. Phys. **67**, 5223 (1990).